3-Pyrazolyl-pyran-2-one: Synthesis, crystal structure, Hirshfeld surface analysis, DFT and ADME studies

Madani Ouhaddou, Latifa Bouissane, Sofia Zazouli, Laurent Jouffret, Abderrafia Hafid, Mostafa Khouili, El Mostafa Ketatni

3-Pyrazolyl-pyran-2-one: Synthesis, crystal structure, Hirshfeld surface analysis, DFT and ADME studies

Madani Ouhaddou,[a] Latifa Bouissane,[a*] Sofia Zazouli,[a] Laurent Jouffret,[b], Abderrafia Hafid,[a] Mostafa Khouili,[a] El Mostafa Ketatni,[a*]

[a] Molecular Chemistry, Materials and Catalysis Laboratory, Faculty of Sciences and Technologies, Sultan Moulay Slimane University, BP 523, Beni-Mellal 23000, Morocco.
[b] Institut de Chimie de Clermont-Ferrand, ICCF-UMR 6296, Université Blaise Pascal, F-63178 Aubière, France.

Correspondence: elm_ketatni@hotmail.fr (ORCID ID 0000-0002-1119-6833)
l.bouissane@usms.ma (ORCID ID: 0000-0002-2231-1956)

Abstract

Synthesis, crystal structure, Hirshfeld surface analysis, DFT and *in-silico* studies were carried out for the 4-hydroxy-6-methyl-3-(1-phenyl-1*H*-pyrazol-3-yl)-2*H*-pyran-2-one **2**. The reaction efficiency was evaluated performing two conditions to prepare the Vilsmeir-Haack reagent: phosphoryl trichloride in DMF and phosphorus pentachloride in DMF. The molecular structure was confirmed by ^{1}H and ^{13}C NMR, IR spectroscopy and X-ray diffraction analysis. The pyrazole and pyran rings are nearly coplanar. The molecules are connected through C—H···O hydrogen bonds, C—H···π and π···π stacking interactions, forming layers in the crystal lattice. Hirshfeld surface analysis for crystal packing indicates that the most important contributions are H···H (41.6%), C···H/H···C (22.6%), O…H/H…O (20.9%) interactions. The frontier molecular orbital, Mulliken and QTAIM atomic charge, Molecular Electrostatic Potential, Natural Bond Orbitals were produced using the optimized structure by B3LYP/6-311G(d,p) level of theory. The calculated LUMO-HOMO gap (4.261 *eV*) indicated that the eventual charge transfer and showed chemical reactivity. Intrinsic reaction coordinate (IRC) calculation confirm that the transition state connects the reactants to the products. The experimental geometry parameters of the title compound are compared with the geometry of the optimized molecule in the gas phase and found in good agreement. The crystal structure was further explored to define the interaction energy between the molecular pairs. The ADME profile that pyrazolyl-pyran-2-one **2** is an inhibitor of CYP1A2 one of the five key cytochrome isoforms enzymes involved in drug metabolism.

Keywords: 3-Pyrazolyl-pyran-2-one; Crystal structure; Hirshfeld surface analysis; DFT; ADME.

1. Introduction

Heterocycles holding pyrazole skeleton are an interesting family of heterocyclic compounds well-known for their numerous biological pharmacological and activities [1] among others antibacterial, antiviral, antiamoebic, antidiabetic, antitumor, anti-inflammatory and antidepressant [1-8]. Several synthetic routes were employed to synthesize the five-membered heterocyclic ring [9]. Commonly, it is obtained proceeding through a tandem condensation-addition sequence [10,11], cycloaddition reactions [12-14] and multicomponent reactions [15]. 3-Acetyl-4-hydroxy-6-methyl-2*H*-pyran-2-one, also known as dehydroacetic acid (DHA), is used as a key intermediate in the synthesis of various heterocycles [16,17], as well as in numerous molecules with pharmacological activities [18,19]. We adopted two different conditions to synthesize 3-pyrazolyl-pyran-2-one **2.** In the first approach, Vilsmeier-Haack conditions were carried out through dehydroacetic acid. In fact, recent studies have reported the cyclization of ketone hydrazones to 1-substituted-4-formylpyrazoles using the *N*-(chloromethylene)-*N*-methylmethanaminium, generated from substituted amide (DMF) and phosphoryl trichloride ($POCl_3$) [20, 21]. In the second approach, we treated (E)-4-hydroxy-6-methyl-3-(1-(2-phenylhydrazineylidene)ethyl)-2*H*-pyran-2-one **1** with phosphorus pentachloride (PCl_5) as the chlorinating agent instead of phosphoryl chloride, [22] **Scheme 1**. This condition seems to be more efficient in the matter of time and yield.

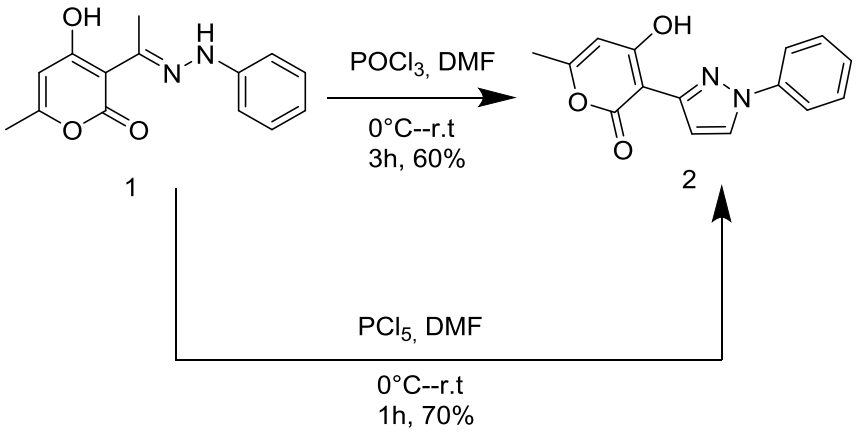

Scheme 1. Synthesis of 3-pyrazolyl-pyran-2-one **2.**

In this current work, we are interested to form the pyrazole ring then investigate the crystal structure of 3-pyrazolyl-pyran-2-one **2**, as well carrying out DFT and ADME (Absorption, distribution, Metabolism, and Excretion) studies to define active sites besides biological application.

2. Experimental

2.1. Reagents and materials

Melting points were measured using a Büchi-Tottoli apparatus. Commercially available reagents were used without further purification. Reactions were monitored by thin layer chromatography (TLC) using aluminium silica gel plates (silica gel 60, F 254 Merck 0.063 – 0.200 mm), and the spots were located with UV light (254 *nm*, 365 *nm*). ^{1}H NMR and ^{13}C NMR spectra were recorded in $CDCl_3$ with TMS as an internal reference using a Bruker AC 500 (1H) or 125 MHz (13C) instruments. Chemical shifts are given in δ parts per million (*ppm*). FTIR analysis was measured from 4000 to 400 cm-1 using Bruker VERTEX 70 FTIR spectrometer with a DTGS detector and OPUS 6.5 software (32 scans at a resolution of 4 cm^{-1}).

2.2. Preparation

Procedure 1: The Vilsmeier-Haack reagent was prepared by reacting DMF (5 ml) and $POCl_3$ (8.52 *mmol*) at 0°C for 30 minutes. Then, hydrazone DHA (**1**) (3.87 *mmol*) was added. The reaction mixture was stirred at 0°C to room temperature for 3 hours. The reaction mixture was poured into ice-cold water and $NaHCO_3$ (5%) was added. The solid was then filtered, washed with water and recrystallized from ethanol leading to 3-pyrazolyl-pyran-2-one **2.** Yield: 60%.

Procedure 2: The Vilsmeier-Haack reagent [22] was prepared by reacting DMF (5 *ml*) and PCl_5 (8.52 *mmol*) at 0°C for 30 minutes. Then, hydrazone DHA (**1**) (3.87 *mmol*) was added. The reaction mixture was stirred at 0°C to room temperature for 1 hour. The reaction mixture was poured into ice-cold water and $NaHCO_3$ (5%) was added. The solid was then filtered, washed with water and recrystallized from ethanol leading to 3-pyrazolyl-pyran-2-one **2**. Yield: 70%.

White solid, mp 173 to 175 °C.^{1}H NMR (500 MHz, $CDCl_3$) δ (*ppm*): 2.25 (s, 3H, CH_3), 6.01 (s, 1H, C5-H, DHA), 7.31-7.27 (m,1H, Ph), 7.35 (d, 1H, C4-H-pyrazole, J = 2.6 Hz), 7.47-7.42 (m, 2H, Ph), 7.60-7.56 (m, 2H, Ph), 7.93 (d, 1H, C5-H-pyrazole, J = 2.6 Hz). ^{13}C-NMR (125 MHz, $CDCl_3$) δ (*ppm*): 20.14 (CH_3), 94.00 (C3-DHA), 101.23 (C5-DHA), 107.91 (C4-pyrazole), 118.92 (C2-Ph), 118.92 (C6-Ph), 127.02 (C4-Ph), 127.40 (C5-pyrazole), 129.76 (C3-Ph), 129.76 (C5-Ph), 139.02 (C1-Ph), 149.40 (C3-pyrazole), 162.05(C6-DHA), 162.74 (C-OH-DHA), 168.72 (C=O-DHA). FTIR: υ cm^{-1}: 3480 (OH), 3100 (C-H arom.), 1720 (C=O), 1600 (C=C Ar), 1520 (C=C Ar), 1370 (CH_3), 1250 (C-O).

2.3. X-ray structure

The X-ray diffraction intensity of pyrazolyl-pyran-2-one **2** was measured at 173K on a Bruker APEX-II CCD diffractometer with MoKα radiation (λ= 0.71073Å). SAINT +6.02 program was used for data collection and reduction [23] and SADABS program was carried out for correction of the absorption effect [24]**.** The structure of pyrazolyl-pyran-2-one **2** was solved by direct methods using SHELXT-2014/5 [25] and refined by full-matrix least-square on F^2 techniques to convergence using the SHELXL-2018/3 program [26]. Non hydrogen atoms were refined with anisotropic displacement parameters. All hydrogen atoms were positioned geometrically and refined using a riding model. The molecular graphic was generated by *Diamond* programs [27].

2.4. Hirshfeld surface analysis and energy framework calculation

The different intermolecular interactions in the crystal packing were quantified with HSA [28] and 2D fingerprint plots [29] using CrystalExplorer version 21.5 [30]. The 3D d_{norm} surfaces were mapped over fixed color scale of –0.1989 to 1.6601a.u., whereas the shape index in the colour range of -1.0 a.u to 1.0 a.u. The HS mapped over the electrostatic potential using *TONTO* with HF/STO-3G level of theory energy in the range of –0.0875 to 0.0633a.u. The intermolecular interaction energies between molecules in pyrazolyl-pyran-2-one **2** were calculated at the B3LYP/6–31G(d,p) level of theory. The enrichment ratio of atomic contacts in crystals is a criterion for predicting the importance of different types of intermolecular interactions [31].

2.5. Computational calculations

Gaussian 09 W software was used to obtain the molecular geometry optimization of pyrazolyl-pyran-2-one **2** and GaussView molecular visualization program [32, 33]. All the quantum chemical based calculations were carried out at the level of DFT/B3LYP/6-311G (d, p) in gas phase [34-36]. The Intrinsic Reaction Coordinate (IRC) analysis was employed to ensure the transition state (TS) optimization method based on the optimized geometries of the reactants and products [37]. The Mulliken charge distribution was analyzed to corroborate the results of the Molecular Electrostatic Potential (MEP). The natural bonding orbitals (NBO) analysis [38] was performed to understand the inter and intra-molecular delocalization or hyperconjugation. QTAIM (Quantum Theory of Atoms in Molecules)

atomic charges was evaluated using Multiwfn software [39] on wave functions generated with Gaussian09 at level of theory as used for NBO analysis. The Molecular Electrostatic Potential was defined to identify the chemical reactive sites. Calculations of ADME properties of pyrazolyl-pyran-2-one **2** were done by using Swiss ADME web server.

3. Results and discussion

3.1. Synthesis

Initially, 4-hydroxy-6-methyl-3-(1-(2-phenylhydrazineylidene)ethyl)-2*H*-pyran-2-one **1** was synthesized through the condensation of phenylhydrazine and DHA, [40] and subsequently underwent the Vilsmeier-Haack reaction, where 2.2 equivalents of PCl_5-DMF reacted with 1 equivalent of hydrazine at 0°C to room temperature for 1h leading to 4-hydroxy-6-methyl-3-(1-phenyl-1*H*-pyrazol-3-yl)-2*H*-pyran-2-one **2** in 70% of yield. The structure of the 3-pyrazolyl-pyran-2-one **2** was established through ^{1}H, ^{13}C NMR and IR spectroscopy, **Fig.S1-S4,** and the single-crystal X-ray diffraction.

Plausible mechanism for formation of the pyrazolyl-pyran-2-one **2** is given below: [41]

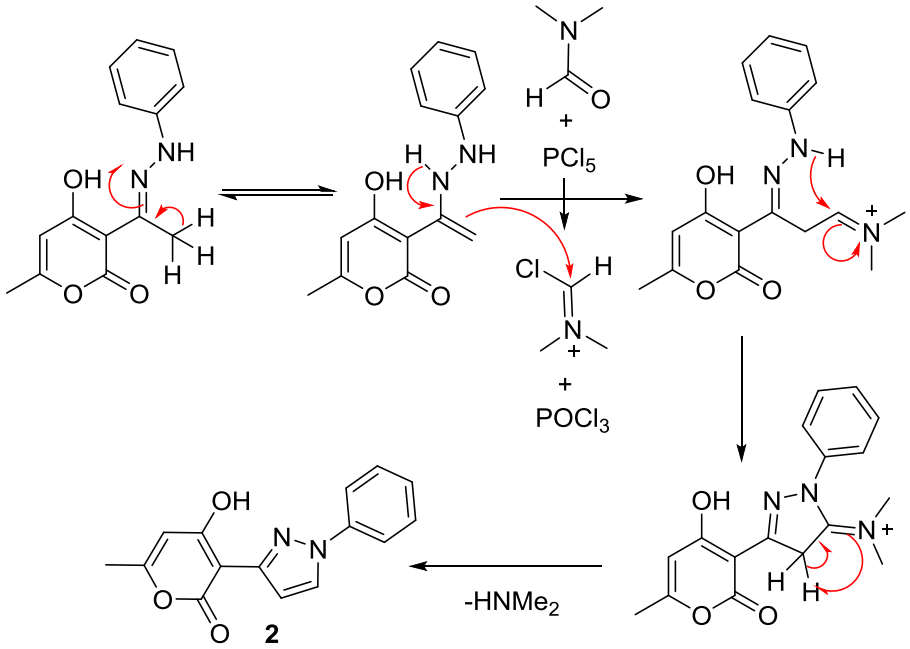

Figure 1. Plausible mechanism for formation of 3-pyrazolyl-pyran-2-one **2.**

3.2. Crystal structure

4-Hydroxy-6-methyl-3-(1-phenyl-1*H*-pyrazol-3-yl)-2*H*-pyran-2-one **2** crystallizes in the monoclinic system with space group $P2_1/c$, **Table S1**. The asymmetric unit of the crystal structure is represented in **Fig.2**. The selected bond distances and angles are reported in **Table S2**. Hydrogen bond distances and angles values are gathered in **Table 1**. The

pyrazole and pyran rings are nearly coplanar with an r.m.s deviation of 0.042 Å. Its mean plane makes a dihedral angle of 18.79(6)° with phenyl ring (C1-C6). The bond lengths for N1-C7 and N2-C9 are 1.354(2) and 1.345(2) Å, respectively, which is similar to the reported structures [42, 43].

The crystal packing of the pyrazolyl-pyran-2-one **2** is stabilized by two intramolecular C8—H8···O2 and O3—H3O···N2 interactions individually makes S(6) ring. In the crystal structure, C—H···O hydrogen bonds link molecules into parallel chains running along [010] (**Fig. 3a**, **Table 1**). An intermolecular C–H···π interaction between the H at C15 and the C1-C6 aromatic ring of the neighboring molecule with H···π distance of 2.66 Å interconnects the molecular chains together (**Table 1** and **Fig. 3b**). In addition, the π-π stacking interactions as observed between the pyrazole and pyran rings (**Fig. 3b**). The dihedral angle between these planes is 2.76(8)° with a distance of 3.358(1)Å. The crystal packing is also stabilized by C—O···π interaction involving carbonyl group and pyrazole ring, with O2···π separation of 3.556(2) Å, as displayed in **Fig. 3b**. Adjacent layers are related by C—H···π, C—O···π and π···π interactions (**Table 1**), leading to the formation of sheets parallel to the (011) plane (**Fig. 3c**). Another significant feature of the crystal packing is a series of strong, inversion related C–H···π, C–O···π interactions and π···π contacts to generate chains of molecules along the c direction. These chains are connected via C6–H6···O2 and C7–H7···O1 contacts to form layers parallel to bc plane (**Fig 3c**).

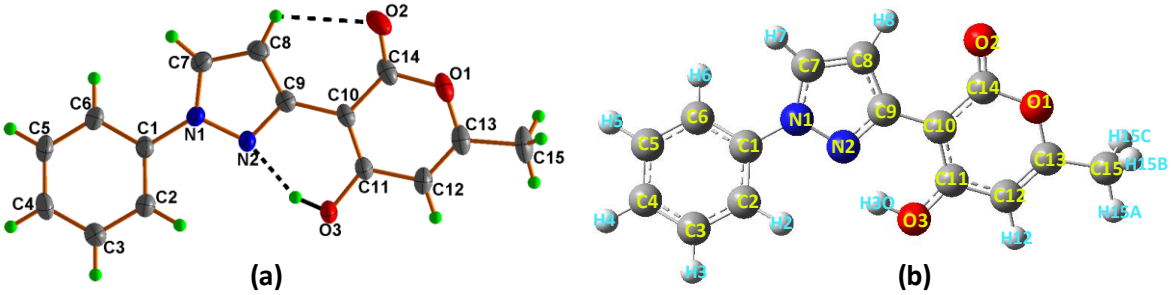

Figure 2. (**a**) Crystal structure with thermal ellipsoids drawn at 50% probability level, the intamolecular hydrogen bonds are shown in the dotted line; (**b**) Optimized structure of pyrazolyl-pyran-2-one **2** obtained by B3LYP/6-311G(d,p).

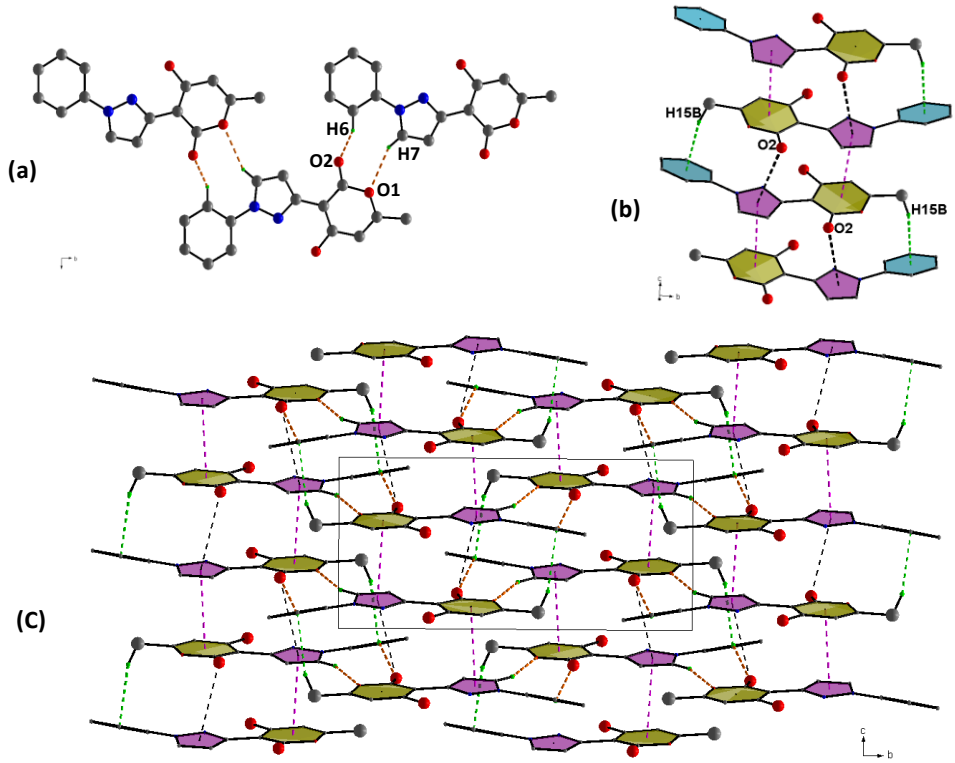

Figure 3. (**a**) C—H···O hydrogen bond interactions in pyrazolyl-pyran-2-one **2**; (**b**) C15—H15B···π, C14—O2···π and π···π interactions and (c) Packing and hydrogen-bonding interactions viewed along the a-axis.

Table 1. Hydrogen bonds (Å, °), C—H···π and π···π interactions for pyrazolyl-pyran-2-one **2**. Cg1, Cg2 and Cg3 represent the centroids of N1/N2/C7-C9, O1/C10-C14 and C1-C6 rings, respectively.

D—H···A	D—H	H···A	D···A	D—H···A	Symmetry codes
O3—H3O···N2	0.86	1.78	2.582(2)	154	
C6—H6···O2	0.95	2.43	3.186(2)	136	1-x, -1/2+y, 1/2-z
C8—H8···O2	0.95	2.45	2.916(2)	110	
C7—H7···O1	0.95	2.65	3.532(2)	154	1-x, -1/2+y, 1/2-z
C15—H15B···Cg3	0.98	2.66	3.587(2)	158	x, 1/2-y, 1/2+z
Cg1···Cg2			3.358(1)		x, 1/2-y, 1/2+z
C14—O2···Cg1			3.556(2)		x, 1/2-y, 1/2+z

3.3. Optimized molecular structure

The optimized molecular structure of pyrazolyl-pyran-2-one **2** obtained by DFT, at the level of 6-311G(d,p), is shown in **Fig. 2b**. Selected Geometric parameters from the X-ray analysis were compared with the theoretical values of the optimized structure and are presented in **Table S2**. The carbonyl C14=O2 bond was seen as 1.206 and 1.205 Å, respectively. In X-ray structure, the C13—O1, C14—O1 and C11—O3 bond lengths are 1.347(2), 1.400(2) and 1.349(2) Å, whereas the calculated values are 1.348, 1.418 and 1.330 Å, respectively.

The value of the double bonds C10=C11 and C12=C13 are 1.391 and 1.351Å which are in agreement with the ones obtained experimentally: 1.368 and 1.335Å, respectively. The two calculated/experimental nitrogen carbon bonds C7—N1, C9—N2 and N1—N2 are illustrated as 1.365 Å /1.341 Å, 1.354Å /1.345Å and 1.354 Å/1.360Å. The C-C bond lengths in phenyl ring were measured in the range of 1.373-1.389 Å by XRD, while the computed values were 1.391-1.397 Å. The correlation values R^2 found by B3LYP/6-311G(d,p) basis set are 0.97 for bond lengths and 0.99 for angles, respectively (**Fig. S5**). The comparison of geometric data points out that the optimized bond lengths and angles correlated with the XRD results.

The IRC (Intrinsic Reaction Coordinate) calculation was performed to confirm whether the transition state is correctly linked to the two minima (reactants and products) (**Fig. 4**). The results of transition states (TS), corresponding to the two attack modes $POCl_3$ and PCl_5, are summarized in **Table S3**. These TSs were confirmed by the presence of a unique imaginary frequency. The reaction energy of the reverse barrier was calculated as 38.906 and 29.493 *kcal/mol* in $POCl_3$ and PCl_5, respectively. It can be seen that the reaction energy barrier was not very high, which means that the product could be easily produced. In this current work we have proved that the attack on the phosphoryl trichloride ($POCl_3$) is kinetically more favourable considering the very high value of the ratio of the velocity constants of the two attack mode $K(POCl_3)/K(PCl_5)$. The structure of transition state is a five-membered ring as depicted in **Fig. S6**. The only imaginary frequenciy of $POCl_3$-TS correspond to the newly formed N1···C7 bond.

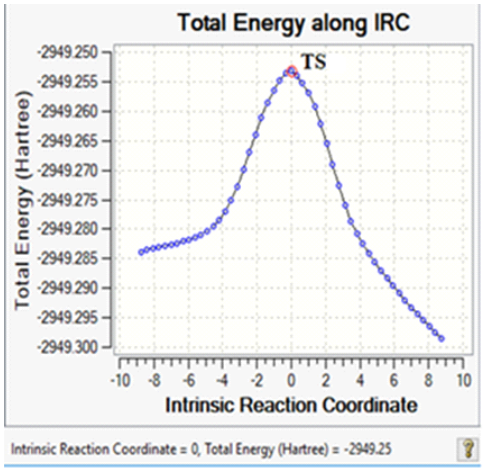

The IRC between N-(chloromethylene)-N methylmethanaminium and phosphoryl trichloride ($POCl_3$)

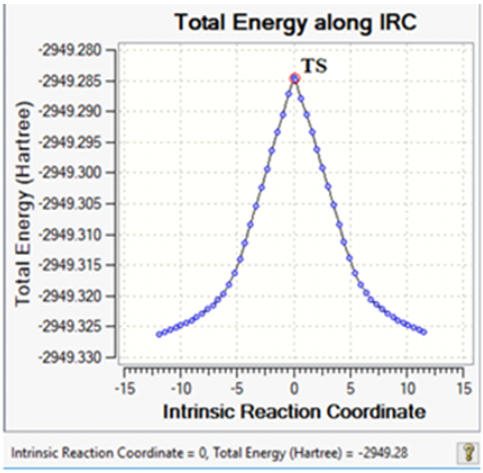

The IRC between N-(chloromethylene)-N methylmethanaminium and phosphorus pentachloride ($PCl5$)

Figure 4: Intrinsic reaction coordinate (IRC) computed at B3LYP/6-311G(d,p) level

3.4. Hirshfeld surface analysis

Hirshfeld surface (HS) analysis and two-dimensional fingerprint plots generated using *CrystalExplorer17.5* [32] show various intermolecular interactions in the crystal structure (**Fig. 5a**). The red spot on the Hirshfeld surface indicates the C6—H6···O2 and small spot represent C7—H7···O1, π···π and C—H···π contacts. The electrostatic potential surface showing blue and red regions indicates positive and negative electrostatic potential (**Fig. 5b**). The two-dimensional fingerprint plots given in **Fig. 6**, indicate the intermolecular contacts and their percentage distributions on the Hirschfeld surface (**Table S4**). The crystal packing is dominated by H···H contacts at 41.6%, as widely scattered points of high density due to the large hydrogen content of the molecule with the tip at $d_e = d_i \approx 1.2$ Å. The force effect C···H/H···C (22.6%) is through to arise from C—H···π contacts viewed as the distribution of points in the form of characteristic wings with $d_e + d_i \approx 2.75$ Å (**Figs. 5c** and **6**). The O…H/H…O interactions (20.9%) (**Fig. 6**) in the structure are represented by a pair of sharp spikes $d_e + d_i \approx 2.30$ Å, representing intermolecular C—H···O hydrogen bond. The distribution of points in the $d_e \approx d_i \approx 1.6$ Å range in the fingerprint plot delineated into C···C contacts, points to the existence of π—π stacking interactions between the pyrazole and pyran rings (**Figs. 5d** and **6**) and confirmed by the red and blue triangles on the surface of the shape-index. Further small contributions from other different interatomic contacts to the Hirshfeld surfaces as follows: C···N/N···C, N···O/O···N, N···H/H···N and O···O contacts of the Hirshfeld surface. The large number of H···H, O...H/H...O and C···H/H···C contact suggests that *van der Waals* interactions and hydrogen bonding have a slight directional influence on the crystal packing.

Enrichment ratio was calculated to analyse the intercontacts having higher propensity to form contacts in the crystal packing (**Table S4**). The C—H ···O (E_{OH} = 1.23) and π···π stacking between pyrazole and pyran rings (E_{CC} = 1.32) specify that they are the most enriched. The molecular surface of pyrazolyl-pyran-2-one **2** is also characterized by H···C and H···H contacts corresponding to the enrichment ratios of $E_{CH/HH}$ = 0.90-1.01. The E_{XY} of C ···O and N···C contacts with enrichment ratios of 0.62 and 2.52, respectively, is another reason which can explain the reduced value of E_{CH}.

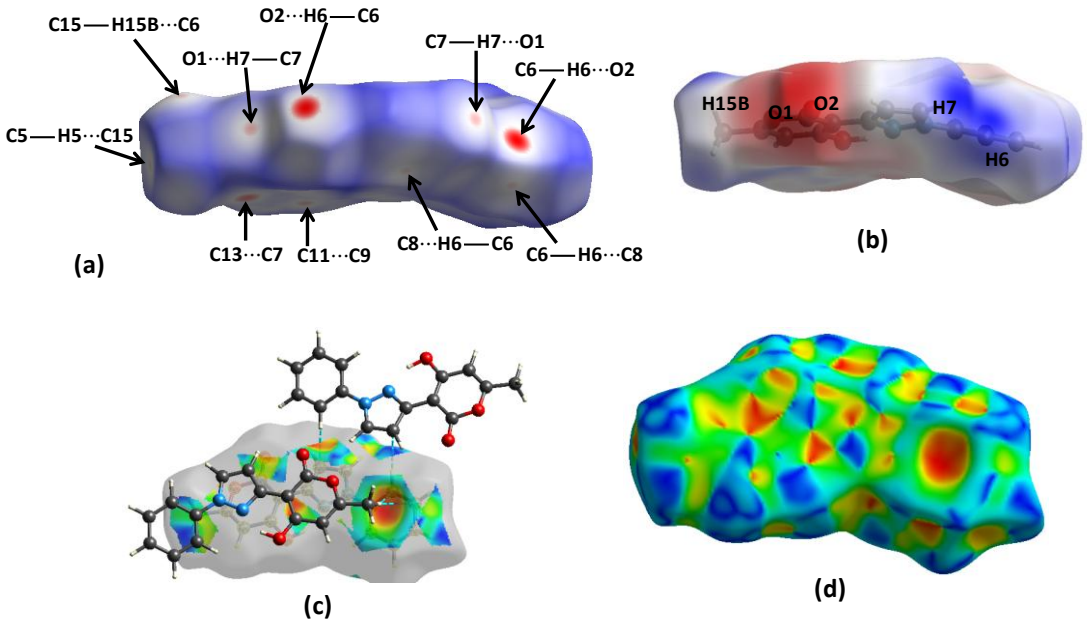

Figure 5. View of the three-dimensional Hirshfeld surface of pyrazolyl-pyran-2-one **2** plotted over (a) d_{norm}, (b) Molecular electrostatic potential, (c) C—H···π interactions and (d) shape-index.

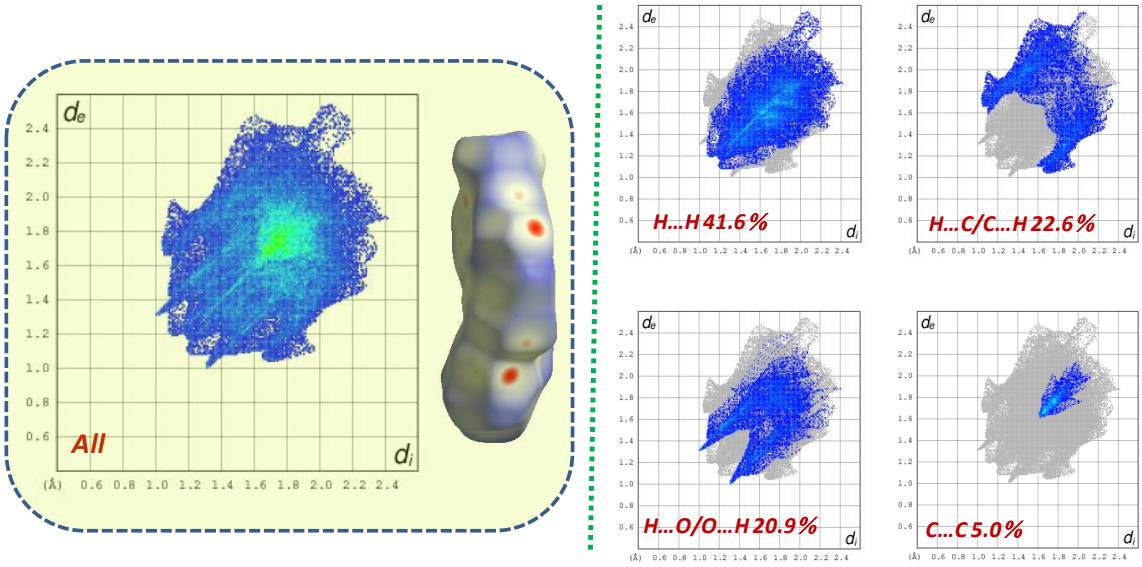

Figure 6. Fingerprint plots of H···H, H···C, H···O and C···C contacts in pyrazolyl-pyran-2-one **2.**

3.5. Void calculation

CrystalExplorer 21.5 software has been used to calculate the voids and their volume in the crystals based on the 0.002 au isosurface (**Fig. 7**). Crystal void calculations computed void volume of 141.61 Å^3 with void area 451 Å^2, asphericity and globularity indices 0.118 and 0.293 units, respectively. The void domain has been found with highest contribution of red coloured domain of surface area 198.01 Å^2 and volume 64.28 Å^3 followed by yellow coloured domain of surface area 188.91 Å^2 and volume 60.66 Å^3. The percentage of crystal

void in unit cell is found to be 11.13%, which indicate the absence of any cavities in the pyrazolyl-pyran-2-one **2**.

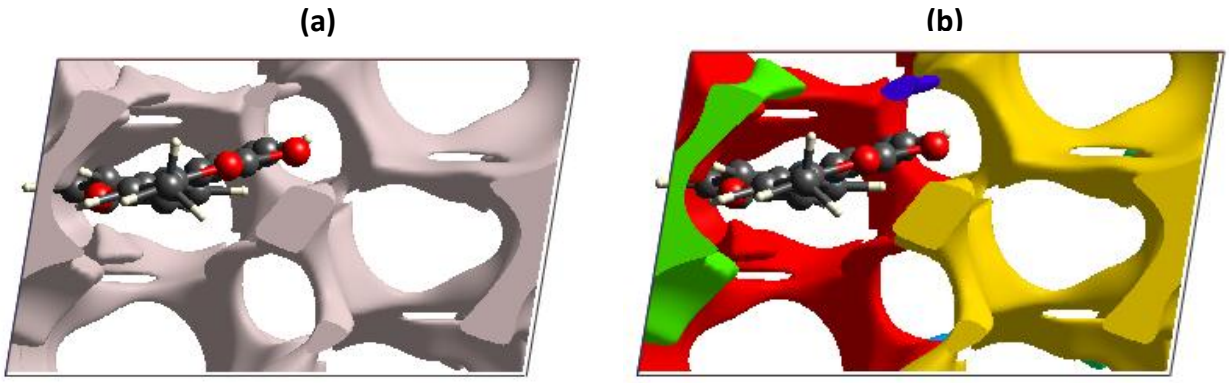

Figure 7. (a) Lattice void and (b) void domain of 3-pyrazolyl-pyran-2-one **2**

3.6. Interaction energy calculations

The interaction energy between molecules in pyrazolyl-pyran-2-one **2** were computed using a B3LYP/6–31G(d,p) energy model available in *Crystal Explorer 17.5* [32], where a cluster of molecules was generated within a radius of 3.8 Å. The total intermolecular energy (E_{tot}) is the sum of electrostatic (E_{ele}), polarization (E_{pol}), dispersion (E_{dis}), and exchange-repulsion (E_{rep}) energies with scale factors of energy framework of k_{ele} = 1.057, k_{pol} = 0.740, k_{dis} = 0.871 and k_{rep} = 0.618. The energy frameworks of pyrazolyl-pyran-2-one **2** were generated for a cluster of 3 × 3 × 3 unit cells to understand the overall topology of the energy distribution in the solid state phase. The interaction energies calculations are represented as cylinders (red for E_{ele}, green for E_{dis} and blue for E_{tot}) that connect centroids of the molecule pairs (**Fig. 8**). **Table 2** describes the interaction energy calculated and visualized in **Fig. 9**. The C15—H15B···π, C14—O2···π and π···π interaction possesses the greatest energy among all close contacts present in the crystal (-54.0 *kJ mol*$^{-1}$), with a major dispersion contribution of -81.8 kJ mol^{-1}. The next most significant contribution, with a total energy of -29.8 *kJ mol*$^{-1}$ and -25.8 *kJ mol*$^{-1}$ correspond to C6—H6···π contacts and C—H···O hydrogen bond, respectively. The attractive dispersion forces play a dominant role in the crystal structure (-187.8 *kJ mol*$^{-1}$). Additionally, the electrostatic, polarization, repulsion and total interaction energies are -66, -18.4, 128.1 and -167.8 *kJ mol*$^{-1}$, respectively.

Table 2. A summary of interaction energies (kJ mol^{-1}) calculated for pyrazolyl-pyran-2-one **2.**

contact	R(Å)	E_{ele}	E_{pot}	E_{dis}	E_{rep}	E_{tot}	Symmetry codes
C15—H15B···π (C1-C6) + π(C10-C14/O1)···π(C7-C9/N1/N2) C14—O2···π (C7-C9/N1/N2)	4.35	-11.0	3.2	-81.8	50.5	-54.0	x, -y+1/2, z+1/2
C6—H6···π (C7-C9/N1/N2)	7.41	-15.6	3.3	-28.1	22.1	-29.8	-x, -y, -z
C6—H6···O2 + C7—H7···O1	9.54	-18.7	5.8	-15.2	18.5	-25.8	-x, y+1/2, -z+1/2

* *R* is the distance between molecular centroids in Å

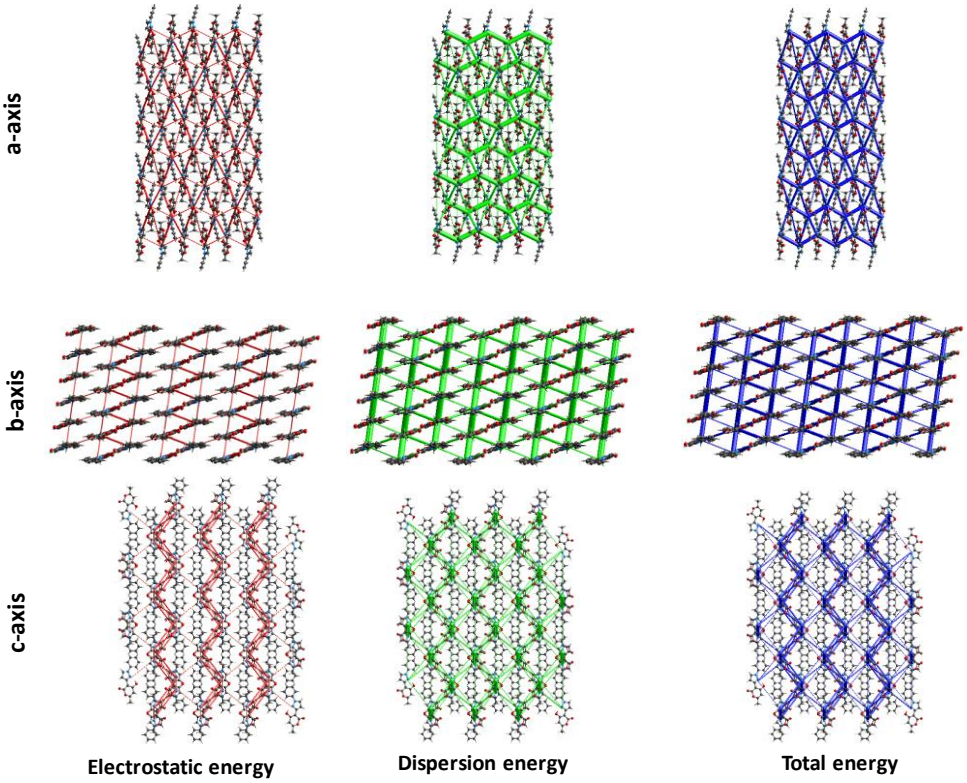

Figure 8. Energy framework of pyrazolyl-pyran-2-one **2**, showing electrostatic, dispersion and total energy force.

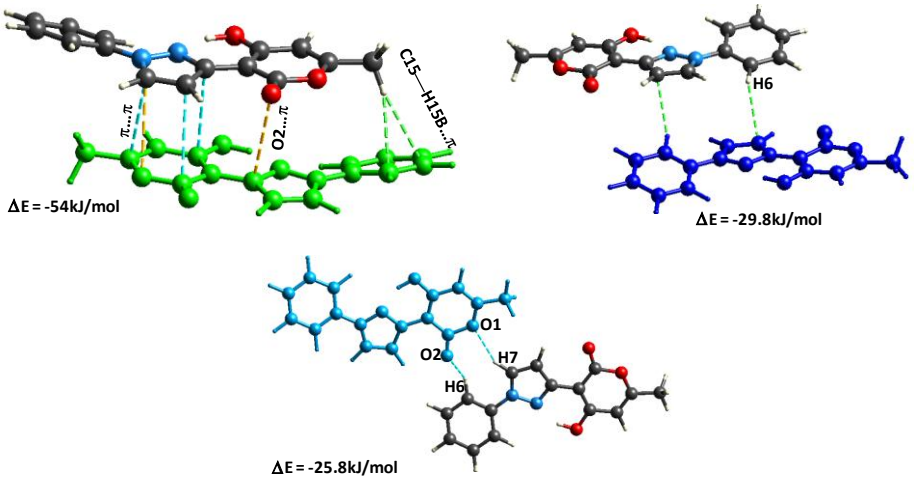

Figure 9. Energetically significant molecular pairs in pyrazolyl-pyran-2-one **2** with their E_{tot} value.

3.7. DFT study

The energy of the HOMO (Highest Occupied Molecular Orbital) is directly related to the ionization potential, while the LUMO (Lowest Unoccupied Molecular Orbital) energy defines the electron-accepting ability of molecule [44-46]. The energy gap between the HOMO and LUMO characterizes the molecular chemical stability**.** The energy levels of the HOMO and LUMO for pyrazolyl-pyran-2-one **2** are depicted in **Fig. 10**. Red and green color distributions represent positive and negative phase in molecular orbital wave function, respectively. The HOMO and LUMO are concerted over the whole molecule. The energies of HOMO and LUMO, energy gap, electronegativity (χ), chemical hardness (η), global softness (ξ) and electrophilicity (ψ) index are presented in **Table 3.** The LUMO-HOMO gap calculated by the B3LYP/6-311G(d,p) is 4.261 *eV*, which indicates that pyrazolyl-pyran-2-one **2** is less reactive and highly stable. The calculated chemical hardness, softness and chemical potential parameters for pyrazolyl-pyran-2-one **2** were found to be 2.130*eV*, 0.235 eV^{-1} and 3.670 *eV*, respectively. The lower gap energy calculated is an indication of a good stability and a high chemical hardness for the studied compound.

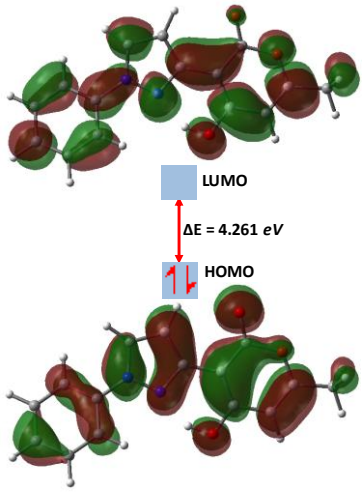

Figure 10. HOMO/LUMO energy gap of pyrazolyl-pyran-2-one **2** at B3LYP/6-311G(d,p).

Table 3. HOMO–LUMO energies and values of quantum chemical parameters calculated by B3LYP/6-311G (d,p)

E_{HOMO} (*eV*)	-5.801
E_{LUMO} (*eV*)	-1.540
$\Delta E_{(LUMO-HOMO)}$ (*eV*)	4.261
Global hardness (η)	2.130
Softness (ξ)	0.235
Chemical potential (μ)	3.670
Electrophilicity (ψ)	3.166
Electronegativity (χ)	-3.670

Dipole moment (D)	3.225

$\eta=1/2[E_{LUMO}-E_{HOMO}]$, $\xi=1/2\eta$, $\mu= -[1/2(E_{LUMO}+E_{HOMO})]$, $\psi= \mu^2/2\eta$, $\chi = -\mu$

3.8. Molecular Properties

3.8.1. Mulliken and QTAIM charges

The Mulliken/QTAIM charges values of pyrazolyl-pyran-2-one **2** were calculated using B3LYP/6-311G(d,p) basis set (**Table 4**). The magnitudes of the atomic charges on carbon atoms were calculated exhibiting positive and negative ranging from -0.403 to 0.450 and -0.033 to 1.341 in Mulliken and QTAIM, respectively. The charge distribution showed that carbon atoms (C1/C7/C9/C11/C13/C14) attached to oxygen/nitrogen atoms have positive charges, while the others carbon atoms showed negative charge in Mulliken except the charge of C8/C12/C15 which is positive in QTAIM. The C14 atom revealed the largest positive charge with ~ 0.450e and 1.341e in Mulliken and QTAIM charges, respectively, due to attachment of the two electronegative O1 and O2 atoms. The low-value negative charge observed for carbons (C2, C3; C4; C5; C6) in the phenyl ring is attributable to the hyperconjugative effect. The H atom attached to the OH group shows a higher positive value (0.277/0.648) compared to other hydrogen atoms. All oxygen and nitrogen atoms possess negative charges values which impose positive charge on carbon atom bonded. The QTAIM molecular graph of pyrazolyl-pyran-2-one **2** is illustrated in **Fig. 11**. It demonstrates the existence of hydrogen donor (O3—H3O and C8—H8) and hydrogen acceptor (N2 and O2) groups, forming a new ring critical point which stabilizes the entire system. However, the presence of intramolecular interactions was identified in the crystal structure.

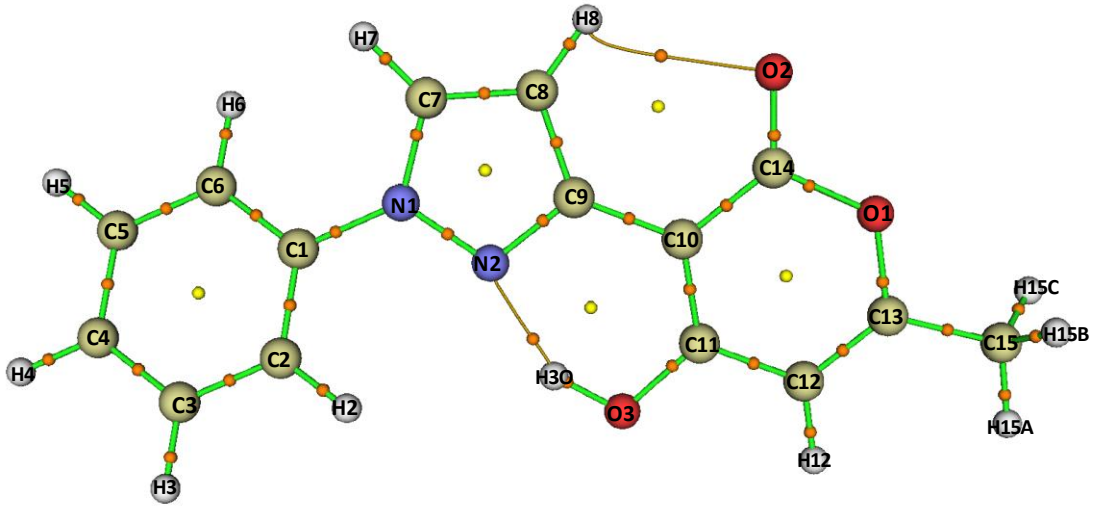

Figure 11. Topological molecular graph of 3-pyrazolyl-pyran-2-one **2**

Table 4: Mulliken and QTAIM charges for pyrazolyl-pyran-2-one **2** using B3LYP / 6-311 g (d, p) levels

Atoms	Mulliken	QTAIM
O1	-0.309	-1.035
O2	-0.333	-1.090
O3	-0.346	-1.141
H3O	0.277	0.648
N1	-0.311	-0.793
N2	-0.405	-0.706
C1	0.207	0.350
C2	-0.059	-0.003
H2	0.121	0.063
C3	-0.098	-0.023
H3	0.103	0.044
C4	-0.084	-0.033
H4	0.100	0.046
C5	-0.097	-0.013
H5	0.101	0.031
C6	-0.106	-0.017
H6	0.110	0.041
C7	0.170	0.325
H7	0.115	0.067
C8	-0.285	0.025
H8	0.136	0.118
C9	0.348	0.458
C10	-0.403	-0.022
C11	0.355	0.603
C12	-0.194	0.024
H12	0.111	0.047
C13	0.172	0.513
C14	0.450	1.341
C15	-0.239	0.009
H15A	0.119	0.035
H15B	0.137	0.043
H15C	0.138	0.046

3.8.2. Molecular electrostatic potential

The molecular electrostatic potential is a suitable method to identify the electrophilic and nucleophilic sites, as well as the detection of hydrogen-bonding interactions [47, 48]. The molecular electrostatic potential (MEP) map of the molecule was computed using DFT/B3LYP/6-311G (d, p) and the contour surface map is displayed in **Fig. 12**. The MEP is scaled from -38 to 38 *kcal/mol*, the red and blue-colored regions indicate nucleophile and electrophile regions, respectively and the green region shows neutral potential. The examination of the MEP surface of pyrazolyl-pyran-2-one **2** reveals that the oxygen atom

O2 exhibits the most highly negative electrostatic potential (-36.39 *kcal/mol*). This region is also influenced by the O1 atom (-31.37 *kcal/mol*). Therefore, the atom in this region acts as an electron donor in intermolecular interactions. The Molecular electrostatic potential value over the center of phenyl and pyrazol rings is negative with -7.53 and -8.16 *kcal/mol*, respectively. The **Fig. 12** reflects C—H···O type intra-inter molecular interactions. The MEP results are supported by the electrostatic contour map positive and negative potential showing the lines isosurface.

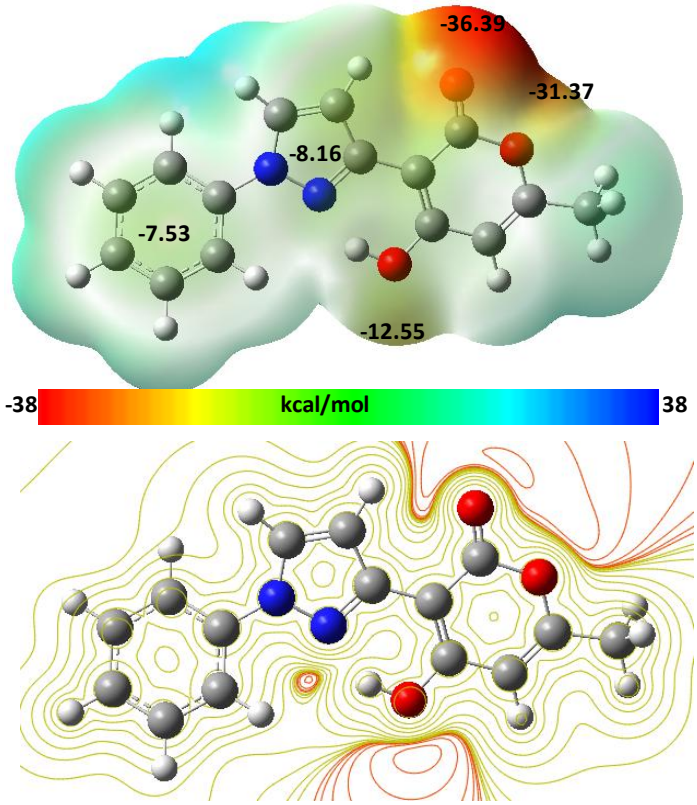

Figure 12. Molecular electrostatic potential and contour map of pyrazolyl-pyran-2-one **2.**

3.8.3. Natural bond orbital analysis

The natural bond orbital analysis has been performed on pyrazolyl-pyran-2-one **2** using B3LYP/6-311g(d,p) method and the results are summarized in **Table 5**. For each donor NBO (*i*) and acceptor NBO (*j*), the stabilization energy $E^{(2)}$ associated with delocalization *i* -> *j* is estimated as [49, 50].

$$E^{(2)} = \Delta E_{ij} = q_i \frac{F(i,j)^2}{E_j - E_i}$$

Where q_i is the donor orbital occupancy, E_i, E_j are the diagonal elements and F_{ij} is the off diagonal NBO Fock matrix element. The larger $E^{(2)}$ values representing the more intensive in the interaction between electron donors and electron acceptors. These results indicate

several transitions π→π*, Lp→σ*, Lp→π* and π*→π for pyrazolyl-pyran-2-one **2**. In fact, the interactions πC2-C3 to π*C1-C6 and π*C4-C5; πC4-C5 to π*C1-C6 and π*C2-C3; πC1-C6 to π*C2-C3 and π*C4-C5 were observed in C1-C6 ring containing stabilization energies of 22.13 and 19.60, 21.22 and 20.29, 20.63 and 18.59 *kcal/mol*, respectively (**Table 5**). Moreover, other transitions are revealed such as πN2-C9 to π*C7-C8; πC7-C8 to π*N2-C9; πC10-C11 to π*O2-C14, π*N2-C9, π*C12-C13 yielding stabilization energies of 10.92, 31.67, 23.39, 9.36, 19.69/20.07 *kcal/mol*, respectively. The stabilization energy $E^{(2)}$ is associated to hyperconjucate interaction from the lone pair of the oxygen atom of carbonyl group LP(2)O2→ σ*(O1-C14) and σ*(C10-C14), oxygen atom of pyran ring LP(2)O1→ π*(O2-C14) and π*(C12-C13) and oxygen atom of OH group LP(2)O3→ π*(C10-C11) with 39.23 and 15.87; 30.21 and 36.50 and 43.49 *kcal/mol*, respectively. Additionally, the highest stabilisation energy containing π*N2-C9→ π*C7-C8 and π*C10-C11 interactions clearly lead to intermolecular charge transfer process in pyrazolyl-pyran-2-one **2**. Higher energy values of E^2 provide more chemical stability in the molecular interaction between electron donors and electron acceptors.

Table 5. Second order perturbation theory analysis of Fock Matrix in NBO Basis for pyrazolyl-pyran-2-one **2** at B3LYP/6-311G (d, p) level.

Donor (i)	ED(i)/e	Acceptor (j)	ED (j)/e	$E^{(2)a}$ *kcal/mol*	E(j)-E(i)[b] *a.u.*
BD(2)N2-C9	1.87337	BD*(2)C7-C8	0.30393	10.92	0.34
BD(2)C1-C6	1.66083	BD*(2)C2-C3	0.32138	18.59	0.30
		BD*(2)C4-C5	0.33476	20.63	0.29
BD(2)C2-C3	1.66939	BD*(2)C1-C6	0.39129	22.13	0.28
		BD*(2)C4-C5	0.33476	19.60	0.28
BD(2)C4-C5		BD*(2)C1-C6	0.39129	20.29	0.27
		BD*(2)C2-C3	0.32138	21.22	0.28
BD(2)C7-C8	1.79476	BD*(2)N2-C9	0.47745	29.13	0.26
BD(2)C10-C11	1.71210	BD*(2)O2-C14	0.33126	31.67	0.29
		BD*(2)N2-C9	0.47745	23.39	0.27
		BD*(2)C12-C13	0.21431	9.36	0.30
BD(2)C12-C13	1.81925	BD*(2)C10-C11	0.35981	20.93	0.31
Lp(2)O1	1.73017	BD*(2)O2-C14	0.33126	30.21	0.35
		BD*(2)C12-C13	0.21431	36.50	0.36
Lp(1)O2	1.97754	RY*(1)C14	0.01611	15.56	1.57
Lp(2)O2	1.82146	BD*(1)O1-C14	0.13327	39.23	0.53
		BD*(1)C10-C14	0.05809	15.87	0.72
Lp(1)O3	1.97195	BD*(1)C10-C11	0.03389	7.95	1.13
Lp(2)O3	1.78801	BD*(2)C10-C11	0.35981	43.49	0.34
Lp(1)N1	1.53310	BD*(2)N2-C9	0.47745	26.73	0.27
		BD*(2)C1-C6	0.39129	24.90	0.29
		BD*(2)C7-C8	0.30393	35.20	0.30
BD*(2)N2-C9	0.47745	BD*(2)C7-C8	0.30393	97.90	0.02

BD*(2)C10-C11	0.35981	117.10	0.02

[a] $E^{(2)}$ means energy of hyper conjugative interaction (stabilization energy)
[b] Energy difference between donor and acceptor i and j NBO orbitals

3.9. *In silico* ADME study

The silico evaluation of the absorption, distribution, metabolism, and excretion (ADME) properties of pyrazolyl-pyran-2-one **2** were carried out by the Swiss ADME web server. Pyrazolyl-pyran-2-one **2**'s SMILE format was uploaded to the online platform to estimate physiological and pharmacokinetic parameters, and the results are shown in **Table 6**. The results showed that pyrazolyl-pyran-2-one **2** can be considered as drug candidates according to Lipinski's rule of five [51], which is an important role in the drug discovery process (molecular weight ≤ 500, octanol-water distribution coefficient logP ≤ 5, hydrogen bond donors ≤ 5 and hydrogen bond acceptors ≤10). In addition, the value of the topological polar surface area (TPSA) of pyrazolyl-pyran-2-one **2** is lower than 140 $Å^2$ which is appropriate and within the prescribed range. Pyrazolyl-pyran-2-one **2** has blood-brain barrier (BBB) permeability and a high gastrointestinal absorption (CI). It does also provide the all other filters, such as Egan [52], Muegge [53] and Ghose [54]. Cytochrome P450 inhibitors are vital liver enzymes that regulate the metabolism of many drugs used in clinical settings. Thus, it is critical to determine if pyrazolyl-pyran-2-one **2** is a cytochrome P450 substrate. Five key cytochrome isoforms enzymes involved in drug metabolism (CYP1A2, CYP2C19, CYP2C9, CYP2D6, and CYP3A4) were investigated (**Table 6**). As a result, it can be concluded that pyrazolyl-pyran-2-one **2** is an inhibitor of CYP1A2 and a no inhibitor for the other isoforms.
ADME parameters GI and BBB were projected in the BOILED-Egg graph as summarized in **Fig. 13**. The yellow region represents the potential BBB permeability, whereas the white area represents the potential GI absorption. In addition, blue dots (PGP+) indicate that P-gp is an active substrate, and red dots (PGP-) indicate that P-gp is not a substrate. The presence of the pyrazolyl-pyran-2-one **2** in the yellow region indicates that it has high brain permeability, and presenting a red dot (PGP-) means that it is not predicted to be a substrate of P-gp. The collected data lead us to conclude that pyrazolyl-pyran-2-one **2** can be an effective therapeutic choice for a targeted disease.

Table 6. Calculated *in silico* ADME parameters of pyrazolyl-pyran-2-one **2**.

Physicochemical properties		**Pharmacokinetics**	
Mol. Wt. (*g/mol*)	268.27	GI absorption	High
No. of heavy atoms	20	BBB permeant	Yes
No. of aromatic heavy atoms	70	P-gp substrate	No
Fraction Csp3	0.07	CYP1A2 inhibitor	Yes
No. of rotatable bonds	2	CYP2C19 inhibitor	No
No. of H-bond acceptors	4	CYP2C9 inhibitor	No
No. of H-bond donors	1	CYP2D6 inhibitor	No
Molar refractivity	74.53	CYP3A4 inhibitor	No
TPSA (Å²)	68.26	Skin permeation (**cm/s**	-6.40
Lipophilicity		**Drug-likeness**	
Log Po/w (iLOGP)	2.54	Lipinski	Yes
Log Po/w (XLOGP3)	2.16	Ghose	Yes
Log Po/w (WLOGP)	2.51	Veber	Yes
Log Po/w (MLOGP)	1.61	Egan	Yes
Log Po/w (SILICOS-IT)	2.47	Muegge	Yes
Consensus Log Po/w	2.26	Bioavailability score	0.55
Water solubility		**Medicinal chemistry**	
Log S (ESOL)	-3.36	PAINS	0 aler
Solubility (*mg/mL; mol/L*)	$1.17\ 10^{-1}$, $4.35\ 10^{-4}$	Brenk	0 aler
Class	Soluble	Lead-likeness	Yes
Log S (Ali)	-3.23	Synthetic accessibility	3
Solubility (*mg/mL; mol/L*)	$1.59\ 10^{-1}$, $5.94\ 10^{-4}$		
Class	Soluble		
Log S (SILICOS-IT)	-4.80		
Solubility (*mg/mL; mol/L*)	$4.29\ 10^{-3}$, $1.60\ 10^{-5}$		
Class	Moderately soluble		

Lipinski(Pfizer) filter: MW≤ 500; MLOGP ≤ 4.15; N or *O* ≤ 10; NH or OH ≤5; Ghose filter: 160 ≤ MW ≤ 480; −0.4 ≤ WLOGP ≤ 5.6; 40 ≤MR ≤130; 20 ≤ atoms ≤ 70; Veber (GSK) filter: Rotatable bonds ≤ 10; TPSA ≤ 140; Egan (Pharmacia) filter: WLOGP ≤ 5.88; TPSA ≤ 131.6; Muegge (Bayer) filter:200 ≤ MW ≤ 600; −0.2 ≤ WLOGP ≤ 5; TPSA ≤ 150; Num. Rings ≤7; Num. Carbon >4; Num. Heteroatoms> 1; Num. Otatable bonds ≤ 15; H-bond acc. ≤ 10; H-bond don. ≤.

A **B**

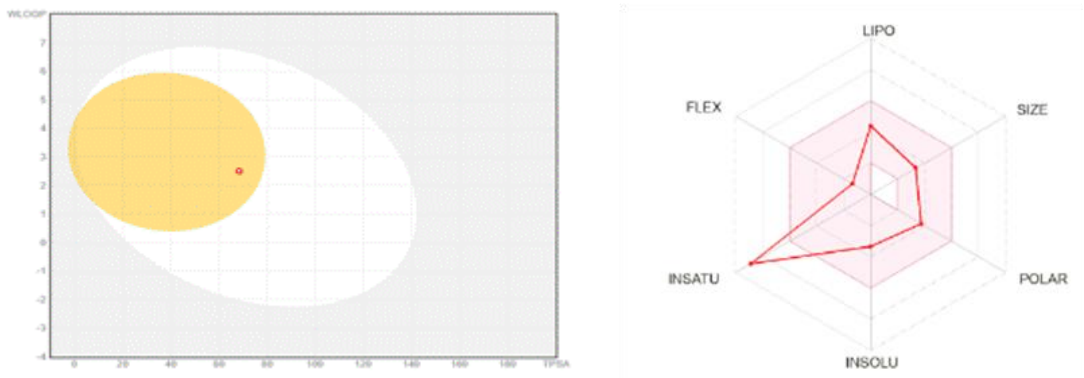

Figure 13. (A) Bioavailability radar and (B) the BOILED-Egg model of pyrazolyl-pyran-2-one **2.**

Conclusion

Pyrazolyl-pyran-2-one **2** was synthesized with good yield (60-70%) using two different conditions to prepare Vilsmeier-Haack reagents. ^{1}H-NMR, ^{13}C-NMR, IR spectroscopy and X-ray diffraction crystallography was performed to elucidate the structure. XRD results revealed that pyrazolyl-pyran-2-one **2** presents monoclinic crystal structure with space group *$P2_1/c$*. This structure is stabilized by C—H···O hydrogen bonding, C—H···π and π ···π interactions. The molecular geometry in the ground state was investigated using DFT methods with 6-311G(d,p) basis set and compared with the experimentally findings. The transition structure for the $POCl_3$ reaction in pyrazolyl-pyran-2-one **2** presented an imaginary frequency with an energy barrier of 38.906 *kcal/mol*. The results of Hirshfeld surface analysis revealed that pyrazolyl-pyran-2-one **2** has a major contribution from H···H, C···H/H···C and O···H/H···O interactions. The dispersion energy was the dominant value among all interaction energies. Additionally, HOMO-LUMO gap was found to be 4.261*eV*. The molecular electrostatic potential show that the electrophilic regions were mainly over the O atom of carbonyl group and in the phenyl and pyrazol ring, while the nucleophilic regions were around the hydrogen atoms. The stability and intermolecular delocalized interactions have been interpreted by NBO analysis. Furthermore, the drug-likeness properties ADME study of pyrazolyl-pyran-2-one **2** were also assessed using ADME analysis, indicating the potential of such compound to be developed as drugs.

Supplementary materials

These data include ^{1}H-^{13}C NMR spectra for pyrazolyl-pyran-2-one **2.** CCDC 2343963 contains the supplementary crystallographic data for compound **2**. These data can be obtained free of charge via www.ccdc.cam.ac.uk/data_request/cif, or by emailing

data_request@ccdc.cam. ac.uk, or by contacting the Cambridge Crystallographic Data Centre, 12 Union Road, Cambridge CB2 1EZ, UK; fax: +44 1223 336033.

Credit author statement

Madani Ouhaddou: Data curation, Writing-original draft. **Latifa Bouissane**: Conceptualization, Methodology, Writing - review & editing. **Sofia Zazouli:** Methodology, Writing-original draft. **Laurent Jouffret**: Methodology, investigation. **Abderrafia Hafid:** Methodology, Investigation. **Mostafa Khouili:** Methodology, Writing-original draft. **El Mostafa Ketatni**: Conceptualization, Methodology, Software, Writing - review & editing. All authors have read and agreed to the published version of the manuscript.

Declaration of Competing Interest

The authors declare that they have no known competing financial interests or personal relationships that could have appeared to influence the work reported in this paper.

Acknowledgements

The authors are thankful to Sultan Moulay Slimane University, Morocco, to the Institut de Chimie de Clermont-Ferrand, Université Blaise Pascal for the X-ray analysis and to National Center for Scientific and Technical Research (CNRST), Morocco, for the NMR analysis. We acknowlege Prof. Mohammed El Idrissi, Faculty Polydisciplinary, Sultan Moulay Slimane University, for his useful co-operation as far as the IRC data.

References

[1] F. Hayat, A. Salahuddin, S. Umar, A. Azam, Synthesis, characterization, antiamoebic activity and cytotoxicity of novel series of pyrazoline derivatives bearing quinoline tail, *Eur.J.Med.Chem.* 45 (2010) 4669-4675.

[2] A.H. Banday, B.P. Mir, I.H. Lone, K.A. Suri, H.M. Kumar, Studies on novel D-ring substituted steroidal pyrazolines as potential anticancer agents, *Steroids* 75 (2010) 805-809.

[3] R.S. Joshi, P.G. Mandhane, S.D. Diwakar, S.K. Dabhade, C.H. Gill, Synthesis, analgesic and anti-inflammatory activities of some novel pyrazolines derivatives, *Bioorg.Med.Chem.Lett.* 20 (2010) 3721-3725.

[4] M. Abid, A. Azam, Synthesis, characterization and antiamoebic activity of 1-(thiazolo[4,5-b]quinoxaline-2-yl)-3-phenyl-2-pyrazoline derivatives, *Bioorg.Med.Chem.Lett.* 16 (2006) 2812-2816.

[5] J.H. Ahn, H.M. Kim, S.H. Jung, S.K. Kang, K.R. Kim, S.D. Rhee, S.D. Yang, H.G. Cheon, S.S. Kim, Synthesis and DP-IV inhibition of cyano-pyrazoline derivatives as potent anti-diabetic agents, *Bioorg.Med.Chem.Lett.* 14 (2004) 4461-4465.

[6] E. Taylor, H. Patel, Synthesis of pyrazolo 3,4-pyrimidine analogues of the potent agent N-4-2-2-amino-4 3H-oxo-7H-pyrrolo 2,3-pyrimidin-5-yl ethylbenzoyl-L-glutamic acid (LY231514), *Tetrahedron* 48 (1992) 8089-8100.

[7] E. Bansal, V.K. Srivastava, A. Kumar, Synthesis and anti-inflammatory activity of 1-acetyl-5-substituted aryl-3-(β-aminonaphthyl)-2-pyrazolines and β-(substitute daminoethyl) amidonaphthalenes, *Eur.J.Med.Chem.* 36 (2001) 81-92.

[8] Y. Rajendra Prasad, A. Lakshmana Rao, L. Prasoona, K. Murali, P. Ravi Kumar, Synthesis and antidepressant activity of some 1,3,5-triphenyl-2-pyrazolines and 3-(2"-hydroxy naphthalen-1"-yl)-1,5-diphenyl-2-pyrazolines, *Bioorg.Med.Chem Lett.* 15 (2005) 5030-5034.

[9] I. Ameziane El Hassani, K. Rouzi, H. Assila, K. Karrouchi, M. Ansar, Recent advances in the synthesis of pyrazole derivatives:A review, *Reactions* 4 (2023) 478–504.

[10] J.W. Sun-Liang Cui, Yan-Guang Wang, Facile Access to pyrazolines via domino reaction of the Huisgen zwitterions with aziridines, *Org. Lett.* 10 (2008) 13-16.

[11] K. Alex, A. Tillack, N. Schwarz, M. Beller, Zinc-catalyzed synthesis of pyrazolines and pyrazoles via hydrohydrazination, *Org. Lett.* 10 (2008) 2377-2379.

[12] A. Suárez, C.W. Downey, G.C. Fu, Kinetic resolutions of azomethine imines via copper-catalyzed [3 + 2] cycloadditions, *J. Am. Chem. Soc.* 127 (2005) 11244-11245.

[13] Y.S. Nathan D. Shapiro, F. Dean Toste, Gold-catalyzed [3+3]-annulation of azomethine imines with propargyl esters, *J. Am. Chem. Soc.* 131 (2009) 11654-11655.

[14] T. Oishi, K. Yoshimura, K. Yamaguchi, N. Mizuno, An efficient copper-mediated 1,3-dipolar cycloaddition of pyrazolidinone-based dipoles to terminal alkynes to produce *N,N*-bicyclic pyrazolidinone derivatives, Chem. Lett. 39 (2010) 1086-1087.

[15] D. Becerra, R. Abonia, J.C. Castillo, Recent applications of the multicomponent synthesis for bioactive pyrazole derivatives, *Molecules* 27 (2022) 4723.

[16] R. Pratap, V.J. Ram, 2*H*-Pyran-2-ones and their annelated analogs as multifaceted building blocks for the fabrication of diverse heterocycles, *Tetrahedron* 73 (2017) 2529-2590.

[17] O. Bouaziz, F. Abboub, N. Bayou-Khier, M. Fodili, P. Hoffmann, M. Amari, Réactivité de l'acide déhydroacétique hydrogené en C5-C6 : Obtention des pyrano-1,5-benzodiazépines différemment substituées et de la structure enaminone, *C. R. Chim.* 15 (2012) 774-778.

[18] Y.B. Li, J. Liu, Z.X. Huang, J.H. Yu, X.F. Xu, P.H. Sun, J. Lin, W.M. Chen, Design, synthesis and biological evaluation of 2-substituted 3-hydroxy-6-methyl-4H-pyran-4-one derivatives as Pseudomonas aeruginosa biofilm inhibitors, *Eur.J.Med Chem.* 158 (2018) 753-766.

[19] L. Saher, M. Makhloufi-Chebli, L. Dermeche, S. Dermeche, B. Boutemeur-Khedis, C. Rabia, M. Hamdi, A.M.S. Silva, 10-(4-Hydroxy-6-methyl-2-oxo-2*H*-pyran-3-yl)-3-methyl-1*H*,10*H*-pyrano[4,3-b] chromen-1-ones from a pseudo-multicomponent reaction and evaluation of their antioxidant activity, *Tetrahedron* 74 (2018) 872-879.

[20] D. Srikrishna, P.K. Dubey, Synthesis of novel substituted 3-(4-((1H-benzo[d]imidazol-2-ylthio)methyl)-1-phenyl-1*H*-pyrazol-3-yl)-2H-chromen-2-ones: various approaches, *Res. Chem. Intermed*. 44 (2018) 4455-4468.

[21] M.A. Kira, M.N. Aboul-Enein, M.I. Korkor, The vilsmeier-haack reaction. IV. Reaction of phosphorus oxychloridedimethylformamide with semicarbazones, *J. Heterocycl. Chem.* 7 (1970) 25-26.
[22] A.H. Romero, Modified procedure for the synthesis of 2-chloroquinoline-3-carbaldehydes using phosphorus pentachloride, *Synth. Commun.* 46 (2016) 287-291.
[23] Bruker, *APEX2* (*SAINT+*), Bruker AXS Inc., Madison, Wisconsin, USA. (2012).
[24] Bruker, *SADABS*. Bruker AXS Inc., Madison, Wisconsin, USA. (2012).
[25] G. M. Sheldrick, SHELXT - Integrated space-group and crystal-structure determination. *Acta Crystallogr.* A71 (2015) 3–8.
[26] G. M. Sheldrick, *SHELXL2018*. University of Göttingen, Germany. (2018).
[27] K. Brandenburg, H. Putz. Diamond. *Cryst. Impact GbR, Bonn, Ger.* (2006).
[28] M. A. Spackman, D. Jayatilaka, Hirshfeld surface analysis, *CrystEngComm.* 11 (2009) 19–32.
[29] J. J. McKinnon, D. Jayatilaka, M. A. Spackman, Towards quantitative analysis of intermolecular interactions with Hirshfeld surfaces. *Chem. Commun.* 37 (2007) 3814–3816.
[30] P. R. Spackman, M. J. Turner, J. J. McKinnon, S. K. Wolff, D. J. Grimwood, D. Jayatilaka, M. A. Spackman, CrystalExplorer: a program for Hirshfeld surface analysis, visualization and quantitative analysis of molecular crystals, *J. Appl. Crystallogr*., 54 (2021), 1006-1011.
[31] C. Jelsch , K. Ejsmont , L. Huder , The enrichment ratio of atomic contacts in crys- tals, an indicator derived from the Hirshfeld surface analysis, *IUCrJ* 1 (2014) 119–128.
[32] M. Frisch, G. W. Trucks, H. B. Schlegel, G. E. Scuseria, M. A. Robb, J. R. Cheeseman, G. Scalmani, V. Barone, B. Mennucci, Ga. Petersson, 'gaussian 09, Revision d. 01, Gaussian', *Inc., Wallingford CT* (2009), 201.
[33] A. Frisch, A. B. Nielson, A. J. Holder, 'Gaussview user manual', *Gaussian Inc., Pittsburgh, PA* 2000, *556*. (2000).
[34] A. D. Becke, Density-functional thermochemistry. III. The role of exact exchange. *J. of Chem. Phys.* 98 (1993) 5648–5652.
[35] C. Lee, W. Yang, R. G. Parr, Development of the Colle-Salvetti correlation-energy formula into a functional of the electron density. *Phys. Rev B.* B37 (1988) 785–789.
[36] B. Miehlich, A. Savin, H. Stoll, H. Preuss, Results obtained with the correlation energy density functionals of becke and Lee, Yang and Parr. *Chem. Phys. Lett.* 157 (1989) 200–206.
[37] Mendez, F., & Gazquez, J. L. Chemical reactivity of enolate ions: the local hard and soft acids and bases principle viewpoint. Journal of the American Chemical Society, 116(20) (1994), 9298-9301
[38] J. Carpenter, F. Weinhold, Analysis of the geometry of the hydroxymethyl radical by the "different hybrids for different spins" natural bond orbital procedure, *Journal of molecular structure*, 169 (1988) 41–62
[39] T. Lu, F. Chen, Multiwfn: A multifunctional wave function analyzer. J. Comp. Chem. 33 (2012) 580-592.
[40] S. Gelin, B. Chantegrel, A. Nadi, Synthesis of 4-(acylacetyl)-1-phenyl-2-pyrazolin-5-ones from 3-acyl-2*H*-pyran-2,4(3*H*)-diones. Their synthetic applications to functionalized 4-oxopyrano[2,3-c]pyrazole derivatives, *J. Org. Chem.* 48 (1983) 4078-4082.
[41] E.A. Ghaith, H.H. Zoorob, M.E. Ibrahim, M. Sawamura, W.S. Hamama, The Scope of 3-acetyl-4-hydroxy-6-methyl-2H-pyran-2-one (DHA), *Curr. Org. Chem.* 24 (2020) 1459-1490.
[42] Y. Laamari, M. Fawzi, M-E. Hachim, B. Abdoullah, A. Oubella, El M. Ketatni, M. Saadi, L. El Ammari, My Y. Ait Itto, H. Morjani, M. Khouili and A. Auhmani, Synthesis, characterization and cytotoxic activity of pyrazole derivatives based on thymol, *Journal of molecular structure*, 1297 (2024) 136864.
[43] M. Chalkha, A. El Moussaoui, T. Ben Hadda, M. Berredjem, A. Bouzina, F. A. Almalki, H. Saghrouchni, M. Bakhouch, M. Saadi, L. El Ammari, M. H. Abdellatiif, M. El Yazidi, Crystallographic study, biological evaluation and DFT/POM/Docking analyses of pyrazole linked amide conjugates: Identification of antimicrobial and antitumor pharmacophore sites, *Journal of molecular structure*, 1252 (2022) 131818.
[44] M. Zia, M. Khalid, S. Hameed, E. Irran, M. M. Naseer, Synthesis and solid state self-assembly of 1,4-diazepine derivative: Water cluster as molecular glue and conformational isomerism, *Journal of molecular structure*, 1207 (2020) 127811.

[45] A. Ali, M. Khalid, M.Abdul Rehman, F. Anwar, H. Zain-Ul-Aabidin, M. N. Akhtar, M. U. Khan, A. A. C. Braga, M. A. Assiri, M. Imran, An Experimental and computational exploration on the electronic, spectroscopic and reactivity properties of novel halo-functionalzed hydrazones, *ACS Omega*, 5 (2020) 18907-18918.

[46] A. Ali, M. Khalid, K. P. Marrugo, G. M. Kamal, M. Saleem, M. U. Khan, O. Concepcion, Spectroscopic and DFT/TDDFT insights of novel phosphonate imine compounds, *Journal of molecular structure*, 1207 (2020) 127838.

[47] C. H. Suresh, G. S. Remya, P. K. Anjalikrishna, Molecular electrostatic potential analysis: a powerful tool to interpret and predict chemical reactivity, *Comput. Mol. Sci.*, 12 (2022), 1-31.

[48] M. Ishwariya, T. Sivaranjani, S. Suresh, S. periandy, S. Soundhariya, Spectroscopic (FT-IR, FT-Raman, NMR and UV–vis), quantum calculation, molecular structure, solvent interaction, ADME and molecular docking investigation on 4-oxo-4h-1-benzopyran-2-carboxylic acid, *Journal of molecular structure*, 1302 (2024) 137452

[49] M. Moumou, F. Outahar, M. Akssira, A. Benharref, M. Saadi, M. Saadi, L. El Ammari, El M. Ketatni, X-ray and DFT calculations of novel spiroisoxazolines derivatives, *Journal of molecular structure*, 1264 (2022) 136324.

[50] M. Khalid, A. Ali, M. Adeel, Z.U. Din, M.N. Tahir, E. Rodrigues-Filho, J. Iqbal, M.U. Khan, Facile preparation, characterization, SC-XRD and DFT/DTDFT study of diversely functionalized unsymmetrical bis-aryl- α, β-unsaturated ketone derivatives, *Journal of molecular structure*. 1206 (2020) 127755,

[51] C. A. Lipinski, F. Lombardo, B. W. Dominy, and P. J. Feeney, "Experimental and computational approaches to estimate solubility and permeability in drug discovery and development settings," *Adv. Drug Deliv. Rev.*, 23, (1997), 3–25.

[52] W. J. Egan, K. M. Merz, and J. J. Baldwin, "Prediction of drug absorption using multivariate statistics," *J. Med. Chem.*, vol. 43, no. 21, (2000), 3867–3877.

[53] I. Muegge, S. L. Heald, and D. Brittelli, "Simple selection criteria for drug-like chemical matter," *J. Med. Chem.*, 44(12), (2001), 1841–1846.

[54] A. K. Ghose, V. N. Viswanadhan, and J. J. Wendoloski, "A knowledge-based approach in designing combinatorial or medicinal chemistry libraries for drug discovery. 1. A qualitative and quantitative characterization of known drug databases," *J. Comb. Chem.*, 1, (1999), 55–68.